A scanning spatial-wavenumber filter and PZT 2-D cruciform array based on-line damage imaging method of composite structure

Lei Qiu[1,2], Bin Liu[3], Shenfang Yuan[1*], Zhongqing Su[2*], Yuanqiang Ren[1]

[1]State Key Lab of Mechanics and Control of Mechanical Structures, Nanjing University of Aeronautics and Astronautics, Nanjing 210016, China.

[2]Department of Mechanical Engineering, The Hong Kong Polytechnic University, Kowloon, Hong Kong

[3]Department of Air Force Military Transportation, Air Force Service College, Xuzhou 221000, China.

***Corresponding author:**

Shenfang Yuan, Email: ysf@nuaa.edu.cn

Zhongqing Su, Email: zhongqing.su@polyu.edu.hk

Abstract: Spatial-wavenumber filtering technique of Lamb wave is gradually studied for damage inspection in recent years because it is an effective approach to distinguish the wave propagating direction and mode. But for on-line damage monitoring of composite structure by using spatial-wavenumber filter, the problem is how to realize the spatial-wavenumber filtering of Lamb wave when the wavenumber response cannot be measured or modeled. This paper proposes a scanning spatial-wavenumber filter and Piezoelectric Transducer (PZT) 2-D cruciform array based on-line damage imaging method of composite structure. In this method, a 2-D cruciform array constructed by two linear PZT arrays is placed on composite structure permanently to obtain Lamb wave damage scattering signal on-line. For one linear PZT array, a scanning spatial-wavenumber filter which does not rely on modeled or measured wavenumber response is designed to filter the damage scattering signal at a designed wavenumber bandwidth to give out a wavenumber-time image. Based on the image, the wavenumber of the damage scattering signal projecting at the array can be obtained. The same process can be also applied to the other linear PZT array to get the wavenumber projecting at that array direction. By combining with the two projection wavenumbers, the damage can be localized without blind angle. The method is validated on an aircraft composite oil tank and the damage localization results are in accordance with the actual damages. It shows an acceptable performance of the damage imaging method for complex composite structure.

Keywords: Structural health monitoring, composite structure, damage imaging, Lamb wave, spatial-wavenumber filter, 2-D cruciform array

1. Introduction

Modern structures on aircraft make increasing use of composite materials. However, the inner damage of composite structure can reduce the strength and even cause air crash [1]. Hence, damage monitoring for composite structure is an important research topic in the field of Structural Health Monitoring (SHM) [1-3].

Among the existing SHM methods for composite structure, much attention has been paid to the Piezoelectric Transducer (PZT) and Lamb wave based SHM technology because it is sensitive to small damage and long detection range, and it can be also applied on-line [1-4]. In recent decade, PZT array and Lamb wave based damage imaging methods have been widely studied, such as delay-and-sum imaging [5-8], time reversal focusing imaging [9-12], damage probability imaging [13-16], ultrasonic phased array [17-20] and multi-signal classification [21]. They utilize a large number of actuator-sensor channels from a network of PZTs to map the structure that was interrogated based on the measurement of Lamb wave damage scattering signal, producing a visual indication of damage location and size, with the advantages of high signal-to-noise ratio, high damage sensitivity and large scale structure monitoring.

However, most of the methods mentioned above process Lamb wave signal in time domain or frequency domain. Comparing with that, the spatial-wavenumber filtering technique performed in spatial-wavenumber domain is an effective approach to distinguish Lamb wave propagating direction and mode. Thus, this technique has been gradually studied and applied to ultrasonic imaging based Non-Destructive Testing (NDT) in recent years [22-27]. In most of these studies, the spatial response of Lamb wave propagating on a inspected structure was measured by using a Scanning Laser Doppler Vibrometer (SLDV) to scan all the spatial measuring points on the whole structure first. Then, 3D Fourier Transform was used to convert the spatial response to wavenumber response. Finally, a wavefield image constructed by the spatial-wavenumber response can be obtained. Based on the wavefield image of the whole structural plane, a spatial-wavenumber filter was set to extract damage features for damage evaluation. Although all these studies showed a high damage inspection accuracy of the spatial-wavenumber filter, they are time-consuming and can be only used to off-line damage inspection because they are limited to point-by-point measurements of Lamb wave spatial-wavenumber response by using the SLDV. It is inconvenient to apply them to on-line damage monitoring.

Considering on-line damage monitoring by taking the advantage of the spatial-wavenumber filtering technique, Purekar et al. [28-29] studied a spatial-wavenumber filter based on-line damage imaging method. In this method, a linear PZT array was placed on a monitored structure permanently to obtain Lamb wave damage scattering signal. But comparing with using the SLDV, the PZT array cannot be moved. It can be only used to obtain the spatial response of the damage scattering signal at the structural area covered by the

PZT array. Therefore, a finite element simulating method was adopted to get the wavenumber of Lamb wave propagating on the structure. After that, a spatial-wavenumber filter was designed based on the modeled wavenumber and the obtained spatial response to search the damage direction. Wang and Yuan [30] also developed this method for damage imaging of composite structure. These previous studies showed a high computational efficiency and damage direction estimation accuracy of the spatial-wavenumber filter. However, the accurate wavenumber response of Lamb wave signal propagating on composite structure is difficult to be modeled, especially on complex composite structure. Therefore, the problem of applying the spatial-wavenumber filter to on-line damage imaging of composite structure is how to realize the spatial-wavenumber filtering of the damage scattering signal when the wavenumber response of Lamb wave cannot be measured or modeled accurately. In addition, the blind angle and near field blindness problem of the linear PZT array should be further studied.

In this paper, a new damage imaging method of composite structure based on a scanning spatial-wavenumber filter and PZT 2-D cruciform array is proposed. The scanning spatial-wavenumber filter which does not rely on only modeled or measured wavenumber response is proposed first. And then, a damage imaging method based on the filter is proposed, and the corresponding damage localization method of no blind angle is given as well. Finally, the method performance for complex composite structure is validated on an aircraft composite oil tank.

2. The scanning spatial-wavenumber filter

In this section, Lamb wave time domain sampling and spatial sampling is given first. Then, the theoretic fundamental of spatial-wavenumber filter is discussed. After that, the scanning spatial-wavenumber filter is proposed.

2.1. Lamb wave time domain sampling and spatial sampling

There is a linear PZTs array placed on a structure as shown in Fig. 1. It consists of M PZTs and the distance between the centers of each two adjacent PZTs is Δx. The PZTs are numbered as m=1,2,…,M. A Cartesian coordinate is built on the array. The center point of the linear PZT array is set to be the original point.

There is a structural damage located at (x_a, y_a). The direction (angle) and distance of the damage relative to the linear PZT array are supposed to be θ_a and l_a respectively. To obtain the damage scattering signal, a frequency narrowband excitation signal of central frequency ω is input to the PZT at the original point to excite Lamb wave of frequency narrowband. When the Lamb wave propagates to the damage, the damage scattering signal is generated and it can be acquired by the linear PZT array. According to some previous studies [4, 9, 17], the amplitude of Lamb wave A_0 mode is dominant at low excitation frequency. Thus, the damage scattering signal can be approximated to be single-mode signal when the excitation frequency is low.

The wavenumber of the damage scattering signal is denoted as k_a. It is wavenumber narrowband and it can be considered as two components. The first component is the wavenumber projecting at the array direction (X-axis projection wavenumber) $k_x=k_a\cos\theta_a$ and the second component is the Y-axis projection wavenumber $k_y=k_a\sin\theta_a$.

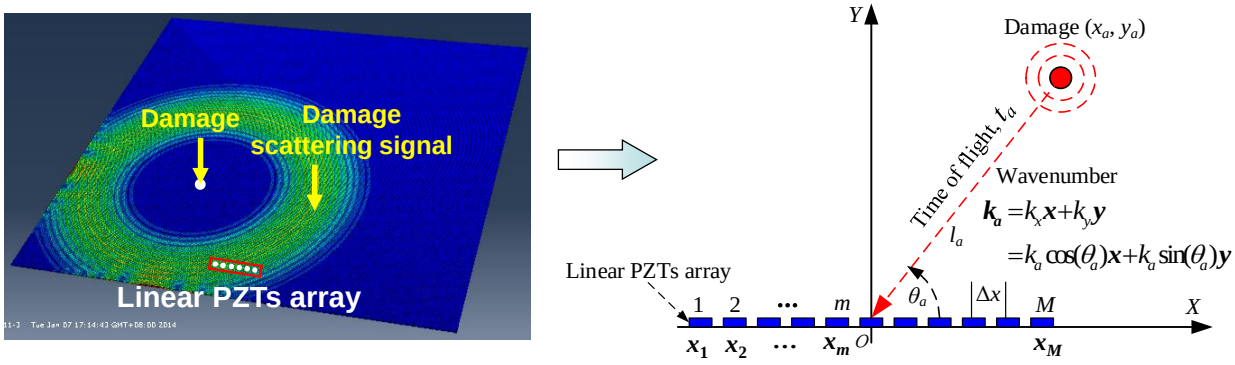

Fig. 1. Schematic diagram of Lamb wave spatial sampling

Fig. 2 gives out an example of the damage scattering signal acquired by a linear PZT array. It is expressed as a waterfall plot. The horizontal coordinate of the figure is sampling time and the Longitudinal coordinate is sampling distance which is corresponding to the location of the PZTs.

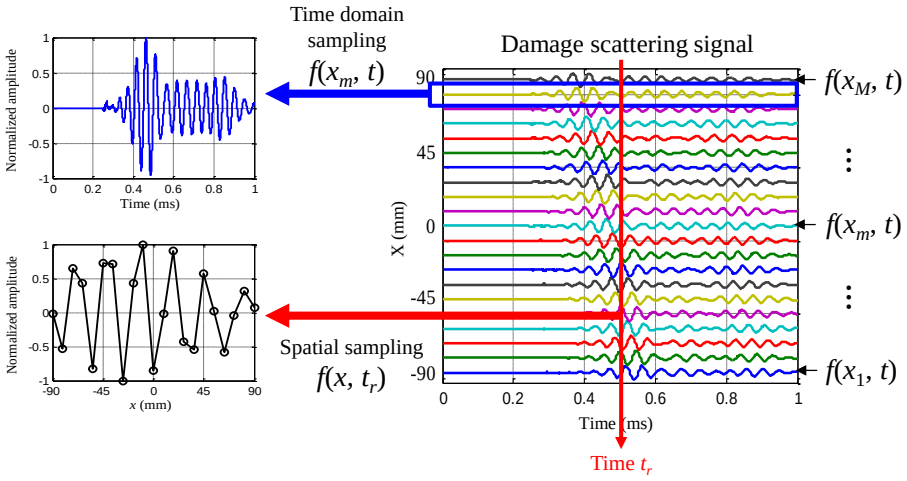

Fig. 2. An example of Lamb wave time domain sampling and spatial sampling

Ordinarily speaking, the linear PZT array is seen to be a time domain sampling device. Each PZT can output a time domain sampling signal as shown in Fig. 2 when looking the waterfall plot from the time direction. The sampling dots (length) and the sampling rate are denoted as L and f_s respectively.

The linear PZT array can be also regarded as a spatial sampling device to acquire spatial response of the damage scattering signal at the area covered by the array when looking the waterfall plot from distance direction. The spatial sampling rate is $2\pi/\Delta x$. The spatial response acquired by the linear PZT array at time t_r can be represented as Eq. (1).

$$f(x,t_r)=\left[f(x_1,t_r),f(x_2,t_r),\cdots,f(x_m,t_r),\cdots,f(x_M,t_r)\right] \tag{1}$$

where $f(x_m, t_r)$ is the damage scattering signal acquired by the PZT located at $(x_m, 0)$ at the time t_r, $x_m=((2m-1)-M)\Delta x/2$. $t_r=r/f_s$ and $r=1,\ldots,L$.

$f(x, t_r)$ is one time spatial sampling of the damage scattering signal at time t_r. Thus, the whole waterfall plot can be seen to be constructed by L times of spatial sampling of the damage scattering signal. Based on this point, the theoretic fundamental of spatial-wavenumber filter is described as the next section.

2.2. The theoretic fundamental of spatial-wavenumber filter

For one time spatial sampling of the damage scattering signal, $f(x_m, t_r)$ can be represented as Eq. (2). In the equation, $u(t_r)$ is the normalized amplitude of the damage scattering signal. $\vec{L}_a$ and $\vec{X}_m$ represent the distance vector of l_a and x_m.

$$f\left(x_m,t_r\right)=u(t_r)e^{i\left(\omega t_r-k_a\left|\vec{L}_a-\vec{X}_m\right|\right)}=u(t_r)e^{i\omega t_r}e^{-ik_a\left|\vec{L}_a-\vec{X}_m\right|} \tag{2}$$

Based on Fraunhofer approximation [31], Eq. (2) can be approximated to be Eq. (3), in which, $\hat{L}_a$ denotes the unit direction vector of the $\vec{L}_a$. In far-field situation, the damage scattering signal can be regarded as a planar wave received by the linear PZT array [31-32]. Thus, Eq. (3) can be approximated to be Eq. (4), in which, $A(t_r)$ denotes the amplitude term and it is expressed as Eq. (5).

$$f\left(x_m,t_r\right)\approx u(t_r)e^{i\omega t_r}e^{-ik_a l_a}e^{ik_a\hat{L}_a\vec{X}_m}e^{-ik_a\frac{x_m{}^2-(\hat{L}_a\vec{X}_m)^2}{2l_a}} \tag{3}$$

$$f\left(x_m,t_r\right)=A(t_r)e^{ik_a\hat{L}_a\vec{X}_m} \tag{4}$$

$$A(t_r)=u(t_r)\cdot e^{i\omega t_r}\cdot e^{-ik_a l_a} \tag{5}$$

By using Fourier Transform, the spatial response shown in Eq. (1) can be transformed to wavenumber response, as shown in Eq. (6), in which, δ is the Dirac function shown in Eq. (7).

$$F\left(k,t_r\right)=\sum_{x=x_1}^{x_M}f\left(x_m,t_r\right)e^{-ikx}=\sum_{x=x_1}^{x_M}A(t_r)e^{ik_a\hat{L}_a\vec{X}}e^{-ikx}=2\pi A(t_r)\cdot\delta(k-k_a\cos\theta_a) \tag{6}$$

$$\delta(k-k_a\cos\theta_a)=\begin{cases}1 & k=k_a\cos\theta_a\\ 0 & k\neq k_a\cos\theta_a\end{cases} \tag{7}$$

It can be seen from Eq. (6) and Eq. (7) that the wavenumber $k_a\cos\theta_a$ of the spatial sampling signal acquired by the linear PZT array is the wavenumber k_a of the damage scattering signal projecting at the X-axis in far-field situation. If the wavenumber k_a can be known beforehand, the damage direction θ_a can be estimated. Thus, a spatial-wavenumber filter can be designed to be Eq. (8) based on the wavenumber k_a [28-30]. In Eq. (8), θ is a searching direction which can be changed from 0° to 180°. The wavenumber response

of the spatial wavenumber filter can be also obtained by using Fourier Transform, as shown in Eq. (9). It indicates that the spatial wavenumber filter has the purpose of selectively passing through the signal of wavenumber $k=k_a\cos\theta$, while rejecting the signal of the other wavenumbers $k\neq k_a\cos\theta$. By applying the spatial-wavenumber filter to the spatial sampling damage scattering signal, the filtered wavenumber response can be expressed as Eq. (10). The symbol '⊗' denotes the convolution operation. It can be noted that if $\theta=\theta_a$, which means that the searching direction of the spatial-wavenumber filter is equal to the damage direction, the amplitude of the filtered response will reach to the maximum value. The damage direction can be estimated correspondingly. This is the original spatial-wavenumber filter [28-30].

$$\phi(x)=\left[e^{i\cdot k_a\cos\theta\cdot x_1},e^{i\cdot k_a\cos\theta\cdot x_2},\cdots,e^{i\cdot k_a\cos\theta\cdot x_m},\cdots,e^{i\cdot k_a\cos\theta\cdot x_M}\right] \tag{8}$$

$$\Phi(k)=\sum_{x=x_1}^{x_M}\mathrm{e}^{ik_a\cos\theta x}\mathrm{e}^{-ikx}=2\pi\delta(k-k_a\cos\theta) \tag{9}$$

$$H(k,t_r)=\sum\left|f(x,t_r)\otimes\phi(x)\right|=\sum\left|4\pi^2\cdot A(t_r)\cdot\delta(k-k_a\cos\theta_a)\cdot\delta(k-k_a\cos\theta)\right| \tag{10}$$

However, the accurate wavenumber k_a must be obtained by modeling or measuring beforehand when using the original spatial-wavenumber filter. It is difficult to be applied to composite structure at current stage. Therefore to promote the spatial-wavenumber filtering technique to be applied to composite structure, a new scanning spatial-wavenumber filter is proposed to solve this problem.

2.3. The scanning spatial-wavenumber filter design

It can be seen from Eq. (8) and (9) that the original spatial-wavenumber filter is designed to search the damage direction directly based on a linear PZT array. Hence, the wavenumber k_a of the damage scattering signal is needed to design the wavenumber of the spatial-wavenumber filter. But as mentioned above, the wavenumber k_a can be considered to be two components including the X-axis projection component and the Y-axis projection component. If the two axis projection wavenumbers can be obtained, the damage direction can be still estimated. Thus, a spatial-wavenumber filter can be designed based on a linear PZT array to search the axis projection wavenumber of the damage scattering not to search the damage direction directly. By using a PZT 2-D cruciform array, this goal can be achieved.

Based on this idea, the scanning spatial-wavenumber filter is designed to be Eq. (11), in which, k_n is the wavenumber of the spatial-wavenumber filter. The corresponding wavenumber response is expressed as Eq.(12).

$$\phi_{k_n}(x)=\left[e^{i\cdot k_n\cdot x_1},e^{i\cdot k_n\cdot x_2},\cdots,e^{i\cdot k_n\cdot x_m},\cdots,e^{i\cdot k_n\cdot x_M}\right] \tag{11}$$

$$\Phi_{k_n}(k)=\sum_{x=x_1}^{x_M}\mathrm{e}^{ik_n x}\mathrm{e}^{-ikx}=2\pi\delta(k-k_n) \tag{12}$$

Fig.3 gives out a basic principle of the scanning spatial-wavenumber filter. k_n is scanned in a wavenumber narrowband from k_1 to k_N, where n=1,…,N, because the damage scattering signal is also wavenumber narrowband. The wavenumber scanning range of k_n is set to be wider than that of the damage scattering signal but it is also limited by the spatial sampling rate. In this paper, k_n=-k_{max}+(n-1)Δk. It is scanned from -k_{max} to +k_{max}. k_{max} is the maximum cutoff wavenumber of the spatial sampling and k_{max}=$\pi/\Delta x$. The wavenumber scanning interval is denoted as Δk. n is also denoted as the scanning step. The maximum scanning step is N=($2k_{max}/\Delta k$)+1.

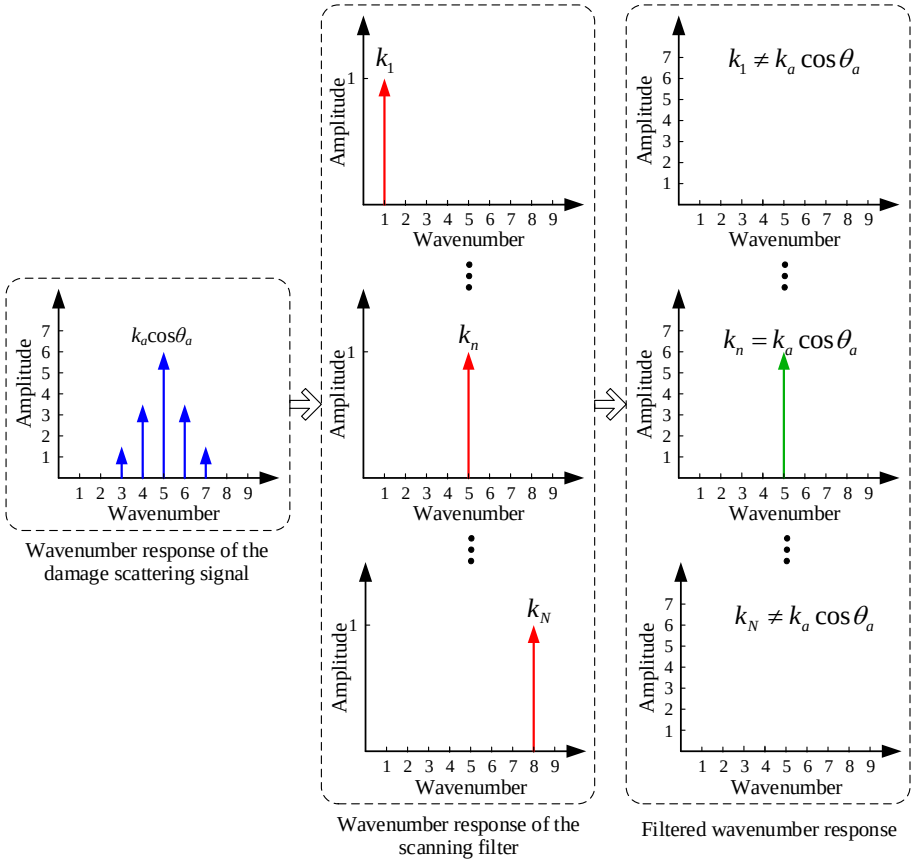

Fig. 3. Schematic diagram of the scanning spatial-wavenumber filter

For a given k_n, a scanning spatial-wavenumber filter can be designed based on Eq. (11) and the amplitude of the filtered response can be calculated by Eq. (13). If k_n=$k_a\cos\theta_a$, which means that the wavenumber of the scanning spatial-wavenumber filter is equal to the X-axis projection wavenumber of the damage scattering signal, the amplitude of the filtered response will reach to the maximum value. Thus, a scanning filtered response vector can be obtained shown in Eq. (14). Fig. 4 shows an example. The spatial sampling signal shown in Fig. 4(a) comes from the waterfall plot shown in Fig.2. The corresponding scanning filtered response is shown in Fig. 4(b) which consists of the filtered response from k_1 to k_N. The wavenumber corresponding to the maximum value can be considered to be the X-axis projection wavenumber.

$$H_{k_n}(k,t_r)=\sum\left|f(x,t_r)\otimes\phi_{k_n}(x)\right|=\sum\left|4\pi^2\cdot A(t_r)\cdot\delta(k-k_a\cos\theta_a)\cdot\delta(k-k_n)\right| \quad (13)$$

$$\boldsymbol{H}(t_r)=[H_{k_1},...,H_{k_n},...,H_{k_N}] \tag{14}$$

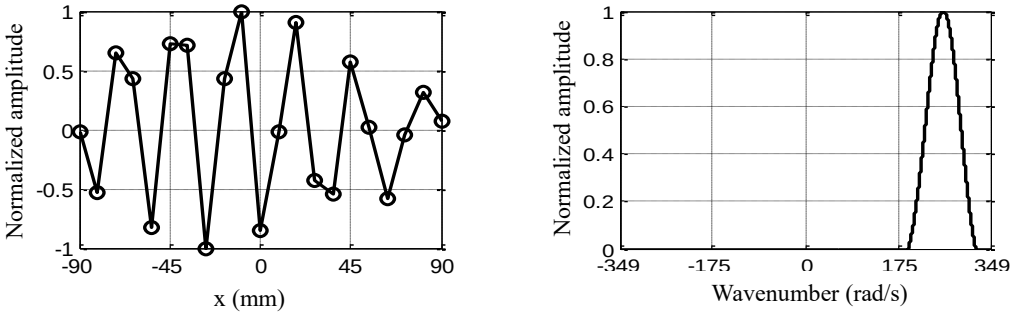

(a) Spatial sampling signal (b) Scanning filtered response

Fig. 4. Example of the scanning spatial-wavenumber filtering result

It should be noted that the scanning spatial-wavenumber filter is realized numerically as shown in Eq.(11) and (13). There is no need to model or measure the wavenumber response of the damage scattering signal. Thus, it can be applied to composite structure easily.

3. The damage imaging and localization method

In this section, the damage imaging method is discussed first. And then, the damage localization method based on PZT 2-D cruciform array is given.

3.1. Damage imaging method based on the scanning spatial-wavenumber filter

As discussed in Section 2.3, a scanning spatial-wavenumber filter can be designed to filter the damage scattering signal of one time spatial sampling at time t_r. It can be also designed to filter the damage scattering signal of L times spatial sampling. This process can be regarded as a time scanning process performed from t_1 to t_L, as shown in Fig. 5(a). Based on the time scanning process, a matrix of the scanning spatial-wavenumber filtering result can be obtained as represented in Eq. (15). Each column of the matrix represents the scanning spatial-wavenumber filtering result at different wavenumber k_n at one time spatial sampling and each row of the matrix represents the filtering result at different time.

$$\mathbf{H}_{L\times N}=\begin{bmatrix}\boldsymbol{H}(t_1)\\ \cdots\\ \boldsymbol{H}(t_r)\\ \cdots\\ \boldsymbol{H}(t_L)\end{bmatrix} \tag{15}$$

Finally, a wavenumber-time image can be generated by imaging the matrix **H**, as shown in Fig. 5(b). In the wavenumber-time image, the wavenumber and the time corresponding to the point of the highest pixel value can be estimated to be the X-axis projection wavenumber $k_n=k_a\cos\theta_a$ and the absolute arrival time t_R of the damage scattering signal respectively. It should be noted that the absolute arrival time is not the actual

time-of-flight of the damage scattering signal. If a 2-D cruciform array constructed by two linear PZT arrays is adopted, the *X*-axis and *Y*-axis projection wavenumbers can be obtained. Combining with the two axis projection wavenumbers and the absolute arrival time, the damage localization of no blind angle can be achieved as given in the next section.

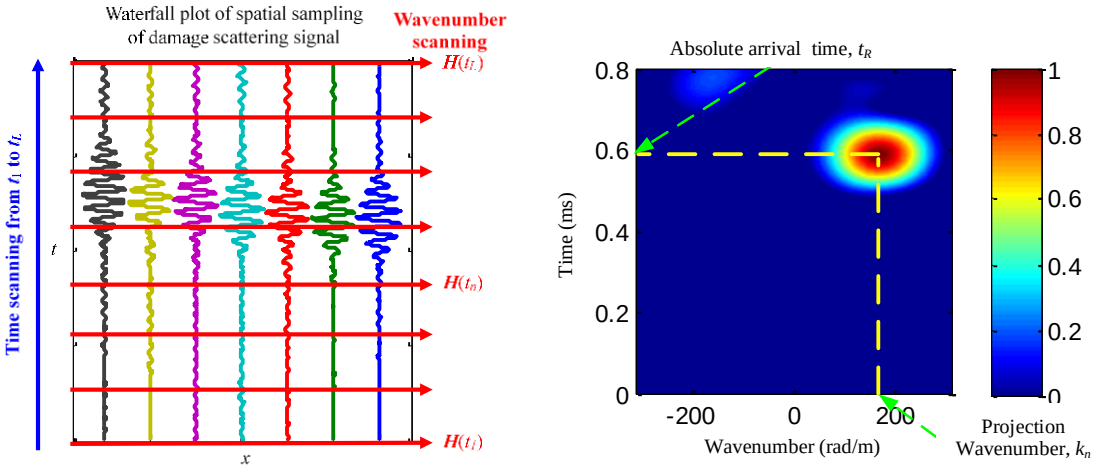

(a) Demonstration of damage imaging process (b) Example of damage imaging result

Fig. 5. Damage imaging process and an example of the imaging result

3.2. Damage localization based on PZT 2-D cruciform array

The 2-D cruciform array is constructed by two linear PZT arrays which are numbered as No.1 and No.2 respectively and they are shown in Fig. 6. The center point of the 2-D cruciform array is set to be the origin point. *X*-axis and *Y*-axis are set to be along with No.1 PZT array and No.2 PZT array respectively. The Lamb wave is excited at the origin point at time t_e. When the damage scattering signal is acquired by the 2-D cruciform array, the axis projection wavenumber and the absolute arrival time (k_{n1}, t_{R1}) of No.1 PZT array and the (k_{n2}, t_{R2}) of No.2 PZT array can be obtained by using the damage imaging method. Then, the damage can be localized by the following method.

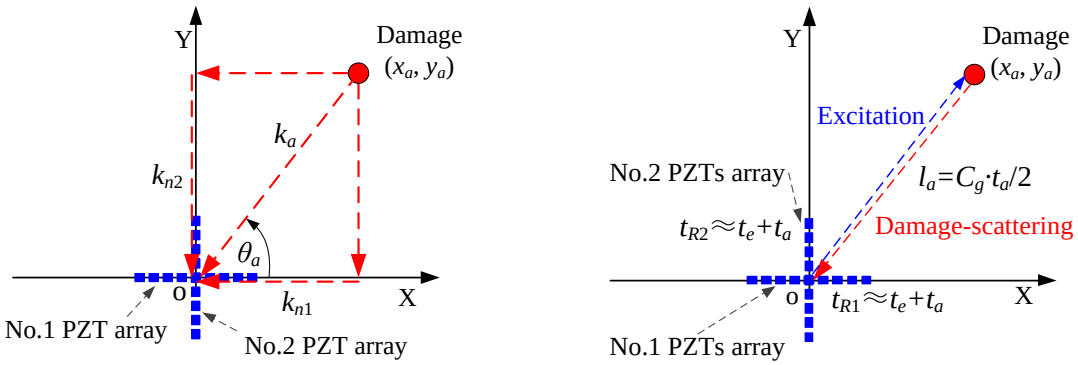

(a) Damage direction estimation (b) Damage distance estimation

Fig. 6. Schematic diagram of damage localization based on the 2-D cruciform array

For damage direction estimation as shown in Fig. 6(a), the wavenumber k_{n1} can be seen to be the *X*-axis

projection wavenumber of k_a and the wavenumber k_{n2} can be seen to be the Y-axis projection wavenumber. They are expressed as Eq. (16). Based on it, the direction θ_a of the damage direction relative to the center point of the 2-D cruciform array can be calculated by Eq. (17). It shows that θ_a can be calculated from 0° to 360° without blind angle.

$$\begin{cases} k_{n1} = k_a \cdot \cos\theta_a \\ k_{n2} = k_a \cdot \sin\theta_a \end{cases} \tag{16}$$

$$\theta_a = \begin{cases} \arctan(\frac{k_{n2}}{k_{n1}}), & (k_{n1} > 0, k_{n2} \geq 0) \\ 90^\circ, & (k_{n1} = 0, k_{n2} > 0) \\ 180^\circ + \arctan(\frac{k_{n2}}{k_{n1}}), & (k_{n1} < 0) \\ 270^\circ, & (k_{n1} = 0, k_{n2} < 0) \\ 360^\circ + \arctan(\frac{k_{n2}}{k_{n1}}), & (k_{n1} < 0, k_{n2} > 0) \end{cases} \tag{17}$$

For damage distance estimation as shown in Fig. 6(b), the absolute arrival time t_R obtained from the wavenumber-time image contains two parts. The first part is the excitation time t_e which can be determined by the excitation signal. The second part is the actual time-of-flight t_a including the time of Lamb wave signal propagating from the excitation position to the damage position and the time of the damage scattering signal propagating back to the 2-D cruciform array. The damage distance l_a relative to the center point of the 2-D cruciform array can be calculated by using Eq. (18) combing with Lamb wave group velocity c_g.

$$\begin{cases} t_R = \dfrac{t_{R1} + t_{R2}}{2} \\ t_a = t_R - t_e \\ l_a = \dfrac{c_g t_a}{2} \end{cases} \tag{18}$$

The final damage position can be obtained by using Eq. (19):

$$\begin{cases} x_a = l_a \cos\theta_a \\ y_a = l_a \sin\theta_a \end{cases} \tag{19}$$

3.3. The implementation process of the damage imaging and localization method

The implementation process of the damage imaging and localization method is summarized as Fig. 7.

(1) In the health state of the structure, the Lamb wave signal acquired by using the 2-D cruciform array is considered to be the health reference signal, f_{HR}. In addition, the Lamb wave group velocity c_g is measured by using wavelet based method [33]. During the on-line damage monitoring process, the acquired Lamb wave signal is the on-line monitoring signals, f_{OM}.

(2) The damage scattering signal is obtained by subtracting f_{OM} from f_{HR}.

(3) For each linear PZT array, the scanning spatial-wavenumber filter is designed and applied to give out a wavenumber-time image based on Eq. (11), (13), (14) and (15). The results of the axis projection wavenumber (k_{n1}, k_{n2}) and the absolute arrival time (t_{R1}, t_{R2}) are obtained.

(4) Based on Eq. (17) and Eq. (18), the damage direction and damage distance are estimated respectively.

(5) Finally, the damage is localized by using Eq. (19).

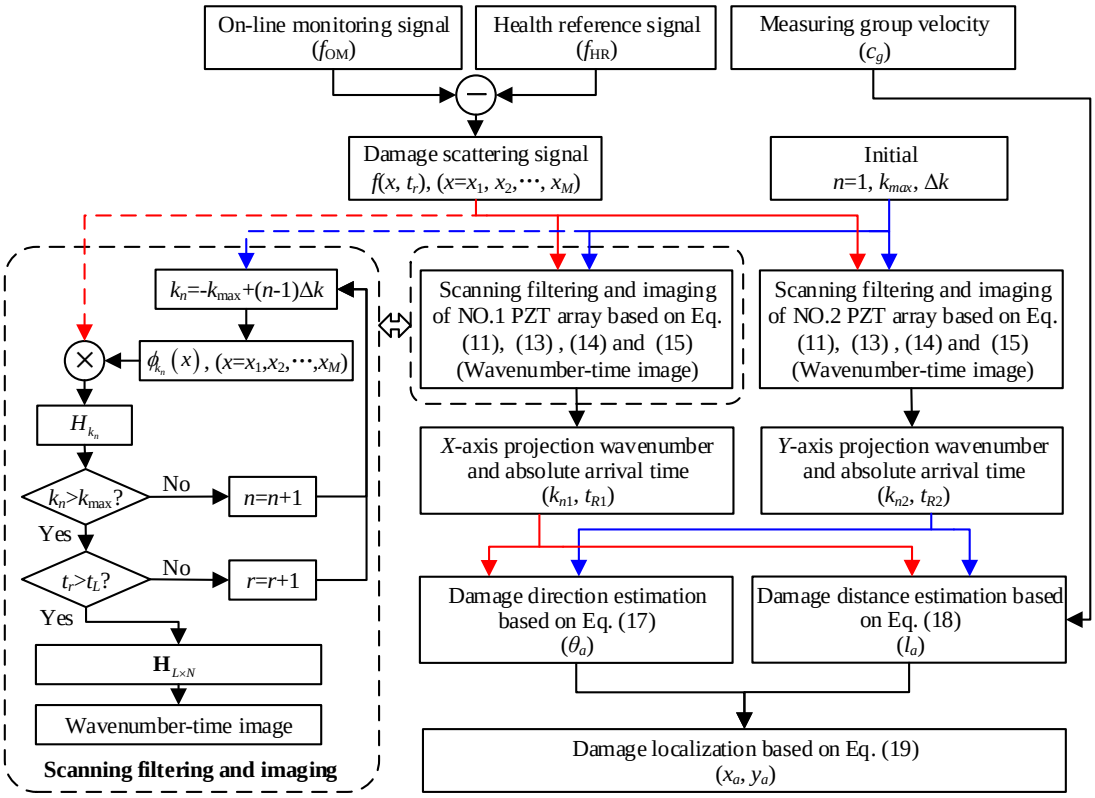

Fig. 7. The implementation process of the damage imaging and localization method

4. Validation of the damage imaging method on an aircraft composite oil tank

4.1. Validation setup

To validate the function and performance of the damage imaging method on complex composite structure, an aircraft composite oil tank is adopted as shown in Fig. 8(a). The dimension of the oil tank is 600mm×300mm×240mm (length×width×height). The composite panel of the oil tank is made of T300/QY8911 carbon fiber and the thickness is variable, as shown in Fig. 9. The central part of the composite panel is the thickest part and it consists of 58 stacked layers. The ply sequence is $[45/0/-45/0/90/0/45/0/-45/0/45/0_2/45/0/-45/0/-45/0_2/45/0/90/0/-45/0/45/0/-45]_s$. The material property of each layer is shown in Table 1. The thickness of each layer is 0.125 mm and the total thickness is 7.25 mm. The thinnest parts are at the two ends and the thicknesses is 4.5 mm.

A 2-D cruciform array is placed on the structure as shown in Fig. 8(b). The distance between the centers of each two adjacent PZTs is Δx=9.0 mm. Thus, the maximum cutoff wavenumber of the linear PZT array is

k_{max}=349 rad/m. Another 3 reference PZT sensors are used to measure the Lamb wave group velocity, and their positions labeled as Ref 1, Ref 2 and Ref 3 are shown in Fig. 8(c) and Table 2.

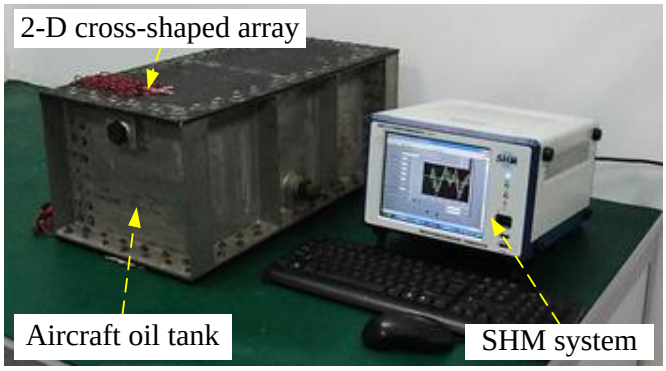

(a) Validation system

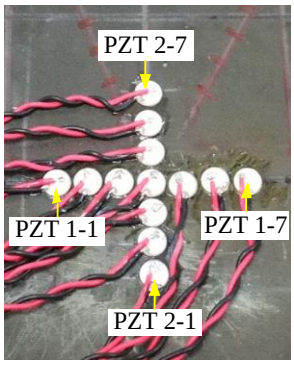

(b) The 2D cross-shaped array

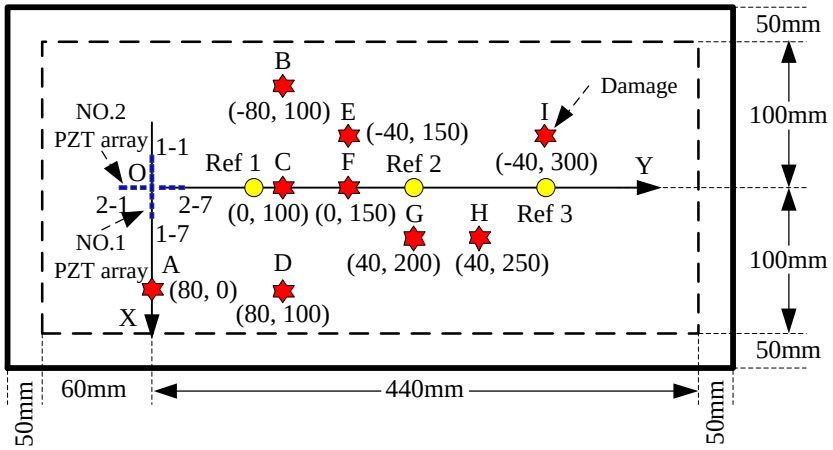

(c) The damage positions and the placement of the 2D cross-shaped array

Fig. 8. Illustration of the performance validation performed on the composite panel of the oil tank

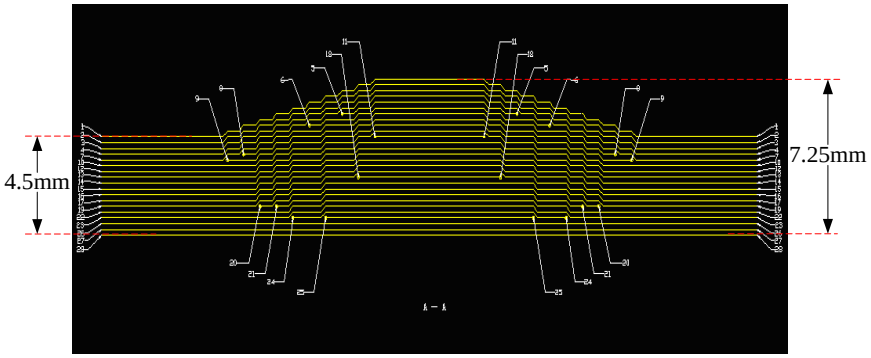

Fig. 9. Variable thickness illustration of the composite panel of the oil tank

Table 1 Material parameters of single layer of the composite panel of the oil tank

Parameter	Value
0° tensile modulus (GPa)	135
90° tensile modulus (GPa)	8.8
±45° in-plane shearing modulus (GPa)	4.47
Poisson ratio μ	0.328
Density (kg·m^{-3})	1.61×10^3

Table 2 The positions of the damages and the reference PZTs on the composite panel of the oil tank

Position label	Cartesian coordinates (mm, mm)	Polar coordinates (°, mm)
Ref 1	(0, 80)	(90.0, 80.0)
Ref 2	(0, 200)	(90.0, 200.0)
Ref 3	(0, 300)	(90.0, 300.0)
A	(80, 0)	(0.0, 80.0)
B	(-80, 100)	(128.7, 128.1)
C	(0, 100)	(90.0, 100.0)
D	(80, 100)	(51.3, 128.1)
E	(-40, 150)	(104.9, 155.2)
F	(0, 150)	(90.0, 150.0)
G	(40, 200)	(78.7, 204.0)
H	(40, 250)	(80.9, 253.2)
I	(-40, 300)	(97.6, 302.7)

9 damages labeled as A to I are simulated on the structure. The positions of these damages are also shown in Fig. 8(c) and Table 2. The damage direction is defined according to counterclockwise direction relative to the positive direction of *X*-axis.

The Lamb wave based SHM system [34] shown in Fig. 8(a) is used to excite and receive Lamb wave signals. The excitation signal is a five-cycle sine burst modulated by Hanning window [8]. The center frequency of the excitation signal is 55 kHz and the excitation amplitude is ±70 volts. The sampling rate is 10 MS/s and the sampling length is 8000 samples including 1000 pre-samples. PZT 2-5 is used to be the Lamb wave actuator for No.1 PZT, and PZT 1-5 is used to be the actuator for No.2 PZT.

The group velocity measuring method based on continuous complex Shannon wavelet transform is used to measure the group velocity. The measuring process is described as follows. (1) The excitation signal is input to the actuator PZT to excite Lamb wave propagating on the composite plate. (2) The corresponding Lamb wave signals of all the 3 reference PZTs are acquired. (3) For each reference PZT, a group velocity can be calculated. The measuring results are $c_{g\text{-}Ref1}$=1485.20 m/s, $c_{g\text{-}Ref2}$=1439.87 m/s and $c_{g\text{-}Ref3}$=1352.27 m/s respectively. (4) Finally, the average group velocity c_g=1425.8 m/s is obtained and it is applied to the following damage localization.

The group velocity measuring method based on continuous complex Shannon wavelet transform is used to measure the group velocity [33]. PZT1-4 is used to excite Lamb wave. The measuring results by using the 3 reference PZTs are $c_{g\text{-}Ref1}$=1695.5m/s, $c_{g\text{-}Ref2}$=1813.8m/s and $c_{g\text{-}Ref3}$=1928.2m/s respectively. Finally, the average group velocity c_g=1812.5m/s is obtained and it is used to the following damage localization.

4.2. Damage imaging validation

The damage E is selected to be an example to show the damage imaging and localization process. The health reference signal f_{HR} and on-line damage monitoring signal f_{OM} are shown in Fig. 10 and Fig. 11 respectively. The damage scattering signal obtained by subtracting f_{OM} from f_{HR} is shown in Fig. 12.

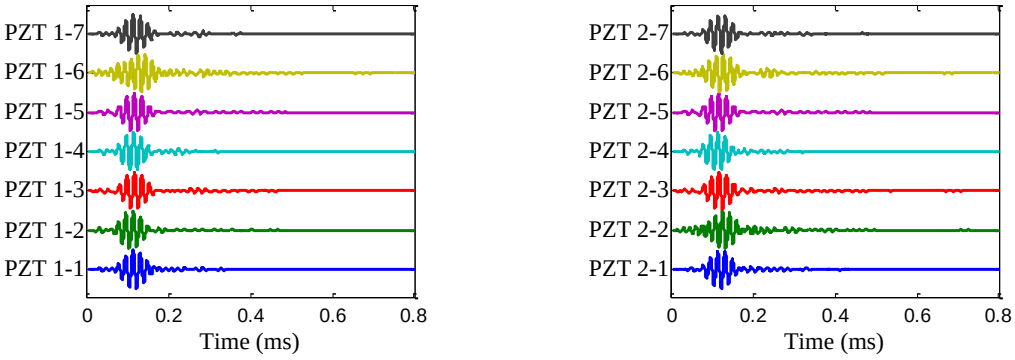

(a) No.1 linear PZT array (b) No.2 linear PZT array

Fig. 10. The health reference signal

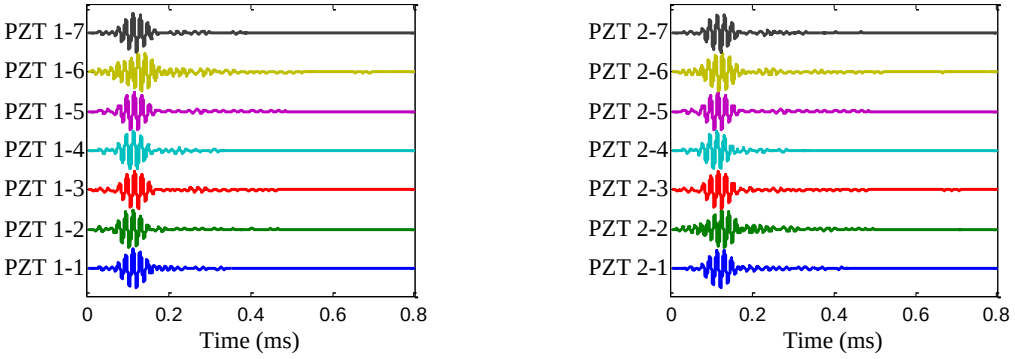

(a) No.1 linear PZT array (b) No.2 linear PZT array

Fig. 11. The on-line damage monitoring signal

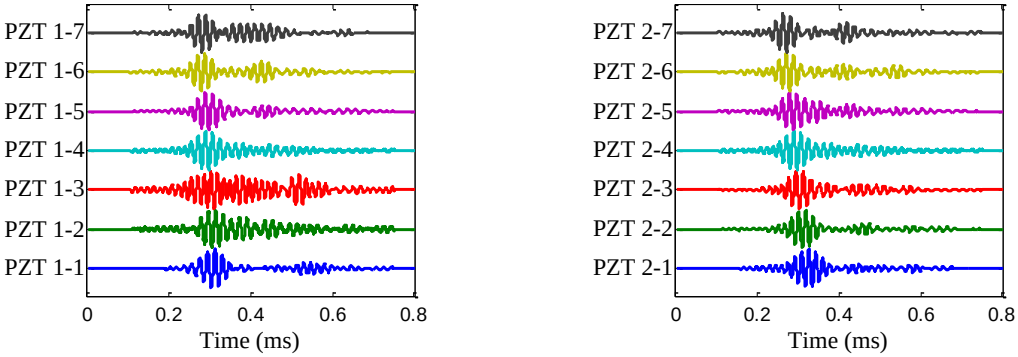

(a) No.1 linear PZT array (b) No.2 linear PZT array

Fig. 12. The damage scattering signal of the damage E

The damage imaging method is applied to the damage scattering signal. The wavenumber scanning range is set to be $-k_{max}$=-349 rad/m to k_{max}=349 rad/m and the wavenumber scanning interval is set to be Δk=1 rad/m. Fig.13 shows the two wavenumber-time images of the damage E.

For damage direction estimation, the axis projection wavenumbers k_{n1}=-87 rad/m and k_{n2}=299 rad/m can be obtained from the two wavenumber-time images. According to Eq. (17), the damage direction is θ_a=106.3°.

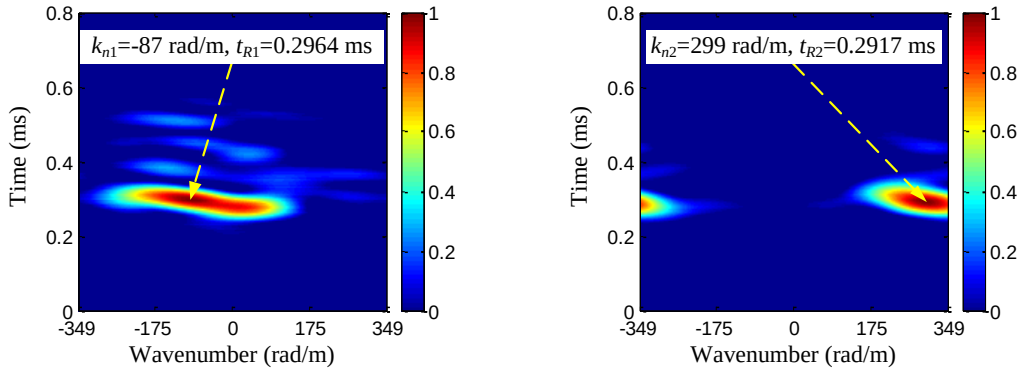

(a) No.1 linear PZT array (b) No.2 linear PZT array

Fig. 13. Damage imaging results of the damage E on the composite panel of the oil tank

For damage distance estimation, the excitation time must be obtained first. The excitation signal is also acquired by the SHM system. By using the continuous complex Shannon wavelet transform [33], the envelope of the excitation signal can be obtained. The time which is corresponding to the maximum value of the envelope is judged to be the excitation time t_e=0.1031ms. The absolute arrival time t_{R1}=0.2964 ms and t_{R2}=0.2917ms can be obtained based on the damage imaging results shown in Fig. 13. According to Eq. (18) and the group velocity c_g=1812.5 m/s, the damage distance is l_a=173.0 mm. Finally, the damage position is obtained to be (-48.5 mm, 166.1 mm) based on Eq. (19), and the damage localization error is Δl=18.2 mm which can be calculated by Eq. (20).

$$\Delta l = \sqrt{(x_a - x_D)^2 + (y_a - y_D)^2} \tag{20}$$

where (x_D, y_D) is the actual position of the damage.

Table 3 Damage localization results of the 9 damages on the composite panel of the oil tank

Damage label	(k_{n1}, t_{R1}) (rad/m, ms)	(k_{n2}, t_{R2}) (rad/m, ms)	Localized position (°, mm)	Actual position (°, mm)	Direction and distance error (°, mm)	Δl (mm)
A	(309, 0.2085)	(1, 0.2059)	(0.1, 94.3)	(0.0, 80.0)	(0.1, 14.3)	14.3
B	(-179, 0.3635)	(238, 0.3590)	(127.1, 138.6)	(128.7, 128.1)	(-1.6, 10.5)	11.2
C	(-1, 0.3227)	(302, 0.3230)	(90.1, 112.4)	(90.0, 100.0)	(0.1, 12.4)	12.4
D	(180, 0.3466)	(241, 0.3428)	(53.2, 137.8)	(51.3, 128.1)	(1.9, 9.8)	10.7
E	(-87, 0.3474)	(299, 0.3417)	(106.3, 173.0)	(104.9, 155.2)	(1.3, 17.8)	18.2
F	(-1, 0.3304)	(305, 0.3293)	(90.1, 158.8)	(90.0, 150.0)	(0.1, 8.8)	8.8
G	(51, 0.3337)	(299, 0.3323)	(80.4, 208.8)	(78.7, 204.0)	(1.7, 4.4)	7.5
H	(38, 0.3340)	(299, 0.3323)	(82.7, 237.7)	(80.9, 253.2)	(1.8, -15.5)	17.4
I	(-40, 0.3389)	(300, 0.3360)	(97.7, 282.4)	(97.6, 302.7)	(0.1, -20.3)	20.3

According to the damage imaging and location process discussed above, the damage localization results and the localization errors of the 9 damages are listed in Table 3. It indicates that the damage localization results are in accordance with the actual damage. For the damage A, it is in the blind angle area of NO.1 PZT array. For the damage C and F, they are in the blind angle area of NO.2 PZT array. But all of them can localized correctly by the imaging and localization method. For the damage I, the Lamb wave excited at the

array must pass through the thickness variable area of the composite panel and the corresponding damage scattering signal also must pass through the thickness variable area when it can be acquired by the array. Thus, the distance estimation error of the damage I is relative larger than the other damages. As it can be seen from the results, the damage localization error is mainly determined by the distance estimation which is limited by the error of the group velocity.

Totally speaking, the damage direction estimation error is less than 2° and the damage distance estimation error is around 20mm. Considering the monitoring area of nearly 600mm×300mm and the variable structural thickness, the damage localization error is acceptable.

5. Conclusion

To promote spatial-wavenumber filtering technique to be applied to on-line damage monitoring of composite structure, this paper proposes a new on-line damage imaging method based on a scanning spatial-wavenumber filter and PZT 2-D cruciform array.

The scanning spatial-wavenumber filter can be designed only according to the maximum cutoff wavenumber of the linear PZT array to scan the actual wavenumber of the damage scattering signal to give out a wavenumber-time image. By using the 2-D cruciform array, the axis projection wavenumbers of the damage scattering signal can be obtained from the two wavenumber-time images and the damage direction can estimated correspondingly without blind angle. According to the absolute arrival time obtained from the wavenumber-time images and combing with the Lamb wave group velocity, the damage distance can be estimated. The method is validated on the composite panel with thickness variable of an aircraft oil tank and the validation results show that that the damage imaging method is feasible to be applied to complex composite structure.

The main contributions and work of this paper is summarized as follows:

(1) For the damage imaging method, there is no need to model or measure the wavenumber response of Lamb wave. Thus, it can be easily applied to on-line damage monitoring of composite structure.

(2) The damage direction can be estimated accurately without blind angle by using the damage imaging method.

(3) The damage imaging and localization on an aircraft composite oil tank is realized.

However, further work should be performed to improve this method including the following three parts:

(1) The method needs the group velocity to achieve damage distance estimation. For damage imaging and localization on complex composite structures, the strong anisotropic feature of the group velocity can introduce large damage localization errors. Therefore, a method which does not rely on the group velocity

should be studied.

(2) The method is based on the far-field situation at the current stage. Though the angle blindness problem is avoided by using the wavenumber scanning and the 2-D cruciform array, the near-field damage monitoring is still a key problem and needs to be studied.

(3) More validations should be performed on complex composite structure.

Funding

This work is supported by the National Science Fund for Distinguished Young Scholars (Grant No.51225502), the Natural Science Foundation of China (Grant No.51205189), State Key Laboratory of Mechanics and Control of Mechanical Structures (Nanjing University of Aeronautics and Astronautics) (Grant No. 0515Y01), the Priority Academic Program Development of Jiangsu Higher Education Institutions and the Hong Kong Scholars Program.

References

[1] C. Boller, F.K. Chang, Y. Fujino, Encyclopedia of structural health monitoring, John Wiley and Sons, Hoboken, New York, 2009.

[2] W.J. Staszewski, S. Mahzan, R. Traynor, Health monitoring of aerospace composite structures-Active and passive approach, Compos. Sci. Technol. 69 (2009) 1678-1685.

[3] K. Lonkar, F.K. Chang, Modeling of piezo-induced ultrasonic wave propagation in composite structures using layered solid spectral element, Struct. Health. Monit. 13 (2014) 50-67.

[4] Z. Su, L. Ye, Identification of damage using lamb waves: from fundamentals to applications, Springer, Berlin, 2009.

[5] J.B. Ihn, F.K. Chang, Pitch-catch active sensing methods in structural health monitoring for aircraft structures, Struc. Health. Monit. 7 (2008) 5-19.

[6] T. Clarke, P. Cawley, P.D. Wilcox, A.J. Croxford, Evaluation of the damage detection capability of a sparse-array guided-wave SHM system applied to a complex structure under varying thermal conditions, IEEE T. Ultrason. Ferr. 56 (2009) 2666-2678.

[7] J.S. Hall, J.E. Michaels, Computational efficiency of ultrasonic guided wave imaging algorithms, IEEE T. Ultrason. Ferr. 58 (2011) 244-248.

[8] L. Qiu, M. Liu, X. Qing, S. Yuan, A quantitative multidamage monitoring method for large-scale complex composite, Struct. Health. Monit. 12 (2013) 183-196.

[9] B. Xu, V. Giurgiutiu, Single mode tuning effects on Lamb wave time reversal with piezoelectric wafer active sensors for structural health monitoring, J. Nondestruct. Eval. 26 (2007) 123-134.

[10] H.W. Park, S.B. Kim, H. Sohn, Understanding a time reversal process in Lamb wave propagation, Wave

Motion. 46 (2009) 451-467.

[11] J. Cai, L. Shi, S. Yuan, Z. Shao, High spatial resolution imaging for structural health monitoring based on virtual time reversal, Smart. Mater. Struct. 20 (2011) 055018.

[12] R. Zhu, G.L. Huang, F.G. Yuan, Fast damage imaging using the time-reversal technique in the frequency-wavenumber domain, Smart. Mater. Struct. 22 (2013) 075028.

[13] D. Wang, L. Ye, Z. Su, Y. Lu, F. Li, G. Meng, Probabilistic damage identification based on correlation analysis using guided wave signals in aluminum plates, Struct. Health. Monit. 9 (2010) 133-144.

[14] C. Zhou, Z. Su, L. Cheng, Quantitative evaluation of orientation-specific damage using elastic waves and probability-based diagnostic imaging, Mech. Syst. Signal. Pr. 25 (2011) 2135-2156.

[15] Z. Wu, K. Liu, Y. Wang, Y. Zheng, Validation and evaluation of damage identification using probability-based diagnostic imaging on a stiffened composite panel, J. Intell. Mater. Syst. Struct. (2014) 1045389X14549873.

[16] J.D. Hua, J. Lin, L. Zeng, High-resolution damage detection based on local signal difference coefficient model, Struct. Health. Monit. 14 (2015) 20-34.

[17] L. Yu, V. Giurgiutiu, In situ 2-D piezoelectric wafer active sensors arrays for guided wave damage detection, Ultrasonics, 48 (2008) 117-134.

[18] C. Holmes, B.W. Drinkwater, P.D. Wilcox, Advanced post-processing for scanned ultrasonic arrays: Application to defect detection and classification in non-destructive evaluation, Ultrasonics, 48 (2008) 636-642.

[19] T. Wandowski, P. Malinowski, W.M. Ostachowicz, Damage detection with concentrated configurations of piezoelectric transducers, Smart. Mater. Struct. 20 (2011) 025002.

[20] F.C. Li, H.K. Peng, G. Meng, Quantitative damage image construction in plate structures using a circular PZT array and lamb waves, Sensor. Actuat. A-Phys. 214 (2014) 66-73.

[21] Y. Zhong, S. Yuan, L. Qiu, Multiple damage detection on aircraft composite structures using near-field MUSIC algorithm, Sensor. Actuat. A-Phys. 214 (2014) 234-244.

[22] M. Ruzzene, Frequency-wavenumber domain filtering for improved damage visualization, Smart. Mater. Struct. 16 (2007) 2116-2129.

[23] T.E. Michaels, J.E. Michaels, M. Ruzzene, Frequency-wavenumber domain analysis of guided wavefields, Ultrasonics, 51 (2011) 452-466.

[24] H. Sohn, D. Dutta, J.Y. Yang, M. DeSimio, S. Olson, E. Swenson, Automated detection of delamination and disbond from wavefield images obtained using a scanning laser vibrometer, Smart. Mater. Struct. 20 (2011) 045017.

[25] M.D. Rogge, C.A. Leckey, Characterization of impact damage in composite laminates using guided wavefield imaging and local wavenumber domain analysis, Ultrasonics, 53 (2013) 1217-1226.

[26] L. Yu, C.A. Leckey, Z. Tian, Study on crack scattering in aluminum plates with Lamb wave frequency-wavenumber analysis, Smart. Mater. Struct. 22 (2013) 065019.

[27] E.B. Flynn, S.Y. Chong, G.J. Jarmer, J.R. Lee, Structural imaging through local wavenumber estimation of guided waves, NDT and E. Int. 59 (2013) 1-10.

[28] A.S. Purekar, D.J. Pines, S. Sundararaman, D.E. Adams, Directional piezoelectric phased array filters for detecting damage in isotropic plates, Smart. Mater. Struct. 13 (2004) 838.

[29] A.S. Purekar, D.J. Pines, Damage detection in thin composite laminates using piezoelectric phased sensor arrays and guided lamb wave interrogation, J. Intell. Mater. Syst. Struct. 21 (2010) 995-1010.

[30] Y. Wang, S. Yuan, L. Qiu, Improved wavelet-based spatial filter of damage imaging method on composite structures, Chinese J, Aeronaut, 24 (2011) 665-672.

[31] C.A. Balanis, Antenna theory analysis and design, John Wiley, Hoboken, 2005.

[32] A. Velichko, P.D. Wilcox, Guided wave arrays for high resolution inspection, J. Acoust. Soc. Am. 123 (2008) 186-196.

[33] L. Qiu, S. Yuan, X. Zhang, Y. Wang, A time reversal focusing based impact imaging method and its evaluation on complex composite structures, Smart. Mater. Struct. 20 (2011) 105014.

[34] L. Qiu, S. Yuan, On development of a multi-channel PZT array scanning system and its evaluating application on UAV wing box, Sensor. Actuat. A-Phys. 151 (2009) 220-230.